Hindawi Publishing Corporation
International Journal of Optics
Volume 2011, Article ID 754610, 11 pages
doi:10.1155/2011/754610

Review Article

Hollow-Core Photonic Crystal Fibers for Surface-Enhanced Raman Scattering Probes

Xuan Yang,[1,2] Chao Shi,[1,2] Rebecca Newhouse,[3] Jin Z. Zhang,[3] and Claire Gu[1,2]

[1] *Department of Electrical Engineering, University of California at Santa Cruz, Santa Cruz, 95064, USA*
[2] *Advanced Studies Laboratories, NASA Ames Research Center, Moffett Field, 94035, USA*
[3] *Department of Chemistry and Biochemistry, University of California at Santa Cruz, Santa Cruz, 95064, USA*

Correspondence should be addressed to Jin Z. Zhang, zhang@chemistry.ucsc.edu and Claire Gu, claire@soe.ucsc.edu

Received 16 September 2010; Revised 27 January 2011; Accepted 8 February 2011

Academic Editor: Wonho Jhe

Photonic crystal fiber (PCF) sensors based on surface-enhanced Raman scattering (SERS) have become increasingly attractive in chemical and biological detections due to the molecular specificity, high sensitivity, and flexibility. In this paper, we review the development of PCF SERS sensors with emphasis on our recent work on SERS sensors utilizing hollow-core photonic crystal fibers (HCPCFs). Specifically, we discuss and compare various HCPCF SERS sensors, including the liquid-filled HCPCF and liquid-core photonic crystal fibers (LCPCFs). We experimentally demonstrate and theoretically analyze the high sensitivity of the HCPCF SERS sensors. Various molecules including Rhodamine B, Rhodamine 6G, human insulin, and tryptophan have been tested to show the excellent performance of these fiber sensors.

1. Introduction

The general demand for sensors for chemical and biological detections is much greater than ever before in various applications, including defense, security, energy, health, industrial pollution, and environmental control. An ideal sensor should possess the following characteristics: high sensitivity, molecular specificity, reliability, stability, low cost, easy fabrication, label-free, short-time detection, reusability, compactness, flexibility, and practicability to a large number of molecular species. In practical applications, most existing sensors can only satisfy some of these requirements, among which high sensitivity and molecular specificity are the two major concerns. Among all the sensors, optical sensors are popular since they are usually very sensitive, non-invasive, and in some cases molecular specific. And the most common optical sensor is fluorescence-based sensor, in which the fluorescence properties of a highly fluorescent molecule (dye, as a label) are changed when it interacts with the analyte of interest [1–4]. The change of luminescence properties of the labeling dye is used as a probe of the analyte. Fluorescence-based scheme provides extremely high sensitivity, low cost, and easy fabrication. However, these types of sensors have one major drawback in that they are generally not molecular specific since the fluorescence spectrum is broad and insensitive to specific molecules.

Comparing to fluorescence spectroscopy, Raman spectroscopy is a powerful optical technique for chemical and biochemical analysis due to its unique molecular specificity [5, 6]. However, it does have one major limitation: the Raman signal is very weak and difficult to detect, especially for samples at low concentrations. To enhance the Raman signal, surface-enhanced Raman scattering (SERS) has been widely employed as an extremely useful spectroscopic tool with both molecular specificity and high sensitivity [7–10]. In SERS, the Raman signal that carries the detailed vibrational information of the molecules can be amplified by orders of magnitude due to strong enhancement of the electromagnetic field by the surface plasmon resonance (SPR) of the metallic nanostructures and the surface chemical enhancement. SERS spectroscopy can provide non-destructive and ultrasensitive detection and identification down to single-molecule level [11, 12], comparable to single-molecule fluorescence spectroscopy while preserving the unique molecular selectivity.

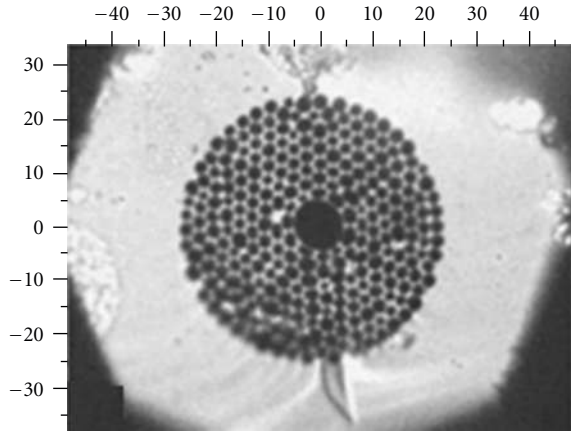

Figure 1: Micrograph of the cross-section of a single HCPCF (scale: μm).

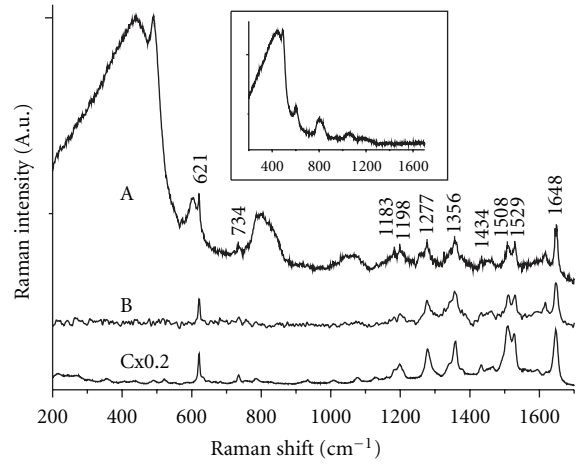

Figure 2: SERS spectra of RhB. Curve A: obtained from the measuring tip of the HCPCF probe (excitation power of ~4.7 mW, scan time of 20 s, and accumulation time of 5). Curve B: a smoothed subtraction between curve A and the HCPCF background (inset). Curve C: obtained using a SERS substrate coated on a Si wafer (excitation power of ~0.47 mW, scan time of 20 s, and accumulation time of 1).

Since its discovery in the 1990s, photonic crystal fibers (PCFs) have emerged as a powerful platform for a multitude of fascinating applications [13–18]. The unique microstructures of axially aligned air channels in PCFs not only provide the photonic bandgap for the confinement of light inside the fiber core, but also offer opportunities for the interaction between the light and the sample, both of which make it a robust and promising platform for optical sensing, including absorption [19, 20], fluorescence [21–23], Raman [24, 25] and SERS [26–37]. In particular, PCF sensors based on SERS are becoming an increasingly attractive sensing technique for various chemical, biological, medical, and environmental detections.

In the past several years, various attempts have been made to employ PCF as a platform for SERS applications. Generally, there are two kinds of PCF sensors based on SERS: one is the solid-core photonic crystal fiber (SCPCF) [26–30] and the other is the hollow-core photonic crystal fibers (HCPCFs) [31–37]. For SCPCF, the cladding holes are usually coated with the SERS substrates (e.g., metal nanoparticles) and filled with the analyte solution, and the Raman signal is generated by the interaction between the evanescent wave and the analyte. For example, Yan et al. reported a SCPCF with four big air holes, surrounding the solid silica core and surface coated with gold nanoparticles for SERS detection [26]. And Amezcua-Correa et al. explored SERS characterization with silver nanoparticles (SNPs) coated on the inner wall of microstructured optical fibers using high-pressure chemical deposition technique [27]. In addition, Du's group has reported a forward-propagating full-length SERS-active SCPCF platform with immobilized and discrete SNPs [28–30].

However, for SCPCFs, the relatively weak evanescent wave may not generate the SERS signal efficiently while most of the light confined inside the central solid core leads to a large Raman background of silica. In contrast, HCPCFs typically have an air core in the center and a periodic structure in the cladding to act as Bragg reflectors. Therefore, the light is well confined in the air core of HCPCFs due to the photonic bandgap (PBG) guiding. In a HCPCF SERS sensor, the sample solution is usually filled into the core (and possibly cladding) channel(s) via capillary effect. As the excitation light interact directly with the sample solution inside the central core, where the electromagnetic field is the strongest, most of the light is utilized for generation of the SERS signal. In addition, as the light is confined inside the hollow core, the interaction between light and silica can be extremely small, which greatly reduces the interference from the fiber background.

In this review, we focus primarily on the recent work from our research labs and aim to illustrate the basic principles of highly sensitive HCPCF sensors based on SERS. Starting with the first integration of HCPCF and SERS substrates, we will review the development of our HCPCF SERS probes, including the liquid-core photonic crystal (LCPCFs), inner wall-coated LCPCF, liquid-filled HCPCF, and modified LCPCF probes.

2. HCPCF SERS Sensors

2.1. HCPCF Probe. The first attempt to combine HCPCF and SERS was carried out in 2006 by Yan et al. [31]. In [31], we presented a HCPCF SERS probe coated with a layer of gold nanoparticles (GNPs) on the inner wall of the air holes. The sample solution entered the air holes due to the capillary effect and then was dried with a heating procedure. The excitation light was coupled into one end, while the SERS substrate and the sample were at the other end of the fiber. After the excitation light propagated in the HCPCF and interacted with the SERS substrate and the molecules, the SERS signal was transmitted back to the measuring tip and then coupled out of the fiber into the Raman spectrometer.

The cross-section of the HCPCF is shown in Figure 1. The central core diameter was around 8 μm, the surrounding

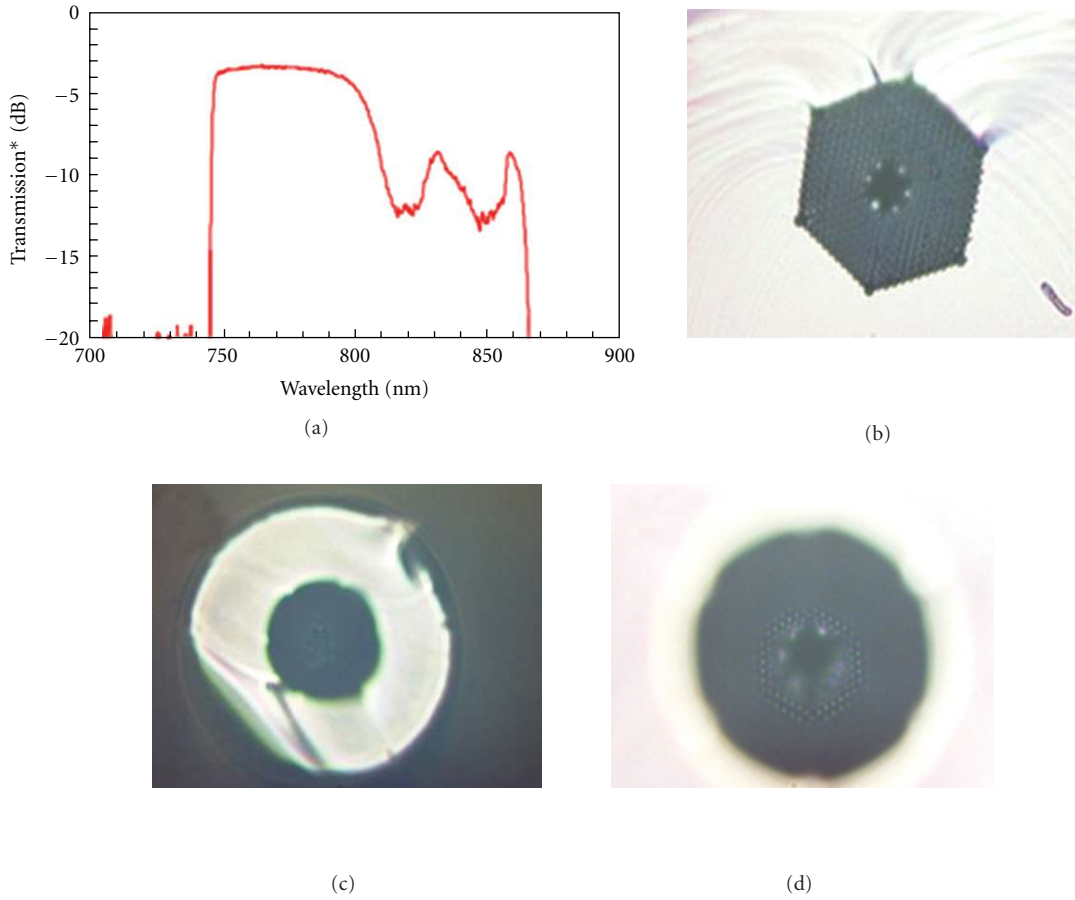

Figure 3: (a) Transmission spectrum of the Air-6 800 photonic crystal fiber (provided by Crystal Fiber). (b) Micrograph of the cross-section of the HCPCF. (c) Probing tip of the HCPCF after postfabrication processing. (d) Enlarged view of (c).

cladding holes diameter was 2.5 μm, and the pitch distance between cladding holes was 3 μm.

The experiment was carried out as follows. A 5 cm HCPCF segment was prepared by cutting carefully at both ends. The Raman background of HCPCF was measured first and its spectrum is shown in the inset of Figure 2, which is the same as that of silica fibers. To coat the GNPs onto the walls of the HCPCF channels, one end of the HCPCF was dipped into the GNPs colloid for 5 min and the solution was drawn up into the holes for about 1–3 cm due to the capillary effect. After a 60°C heating condition for about 2 h, the GNPs were coated on the inner wall of the air holes. With Rhodamine B (RhB, 10^{-5} M) as a test molecule, the coated tip of HCPCF was dipped into the sample solution, then taken out and dried under 60°C heating condition for half an hour. The SERS signal was measured from the other end of HCPCF using a Renishaw Raman System (Renishaw Inc., model: RM2000) with a 632.8 nm excitation light. A 50x objective lens was used to couple the light into the fiber and collect the SERS signal as well.

The SERS spectrum of RhB with the Raman background from the fiber is shown as Curve A in Figure 2. And the SERS signal of RhB with the fiber background removed is shown as Curve B in Figure 2. For reference, curve C in Figure 2

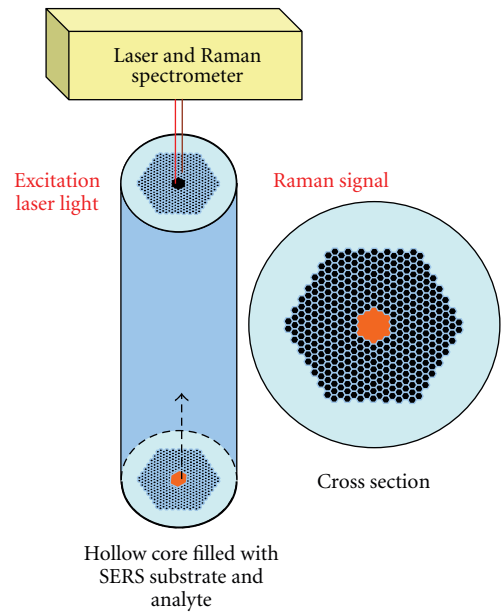

Figure 4: Schematic of the LCPCF SERS sensor and its cross-sectional view. The spectrometer above the surface contains a CCD detector, a monochromator, and electronics for data collection.

shows the SERS spectrum of RhB obtained on a Si Wafer coated with the same GNPs. Almost every characteristic peak in curve B matches that in curve C, which is also consistent with that reported in the literature [38].

This was the first demonstration of combining SERS effect and HCPCF platform together. However, this kind of HCPCF probe can only work well when the sample solution is dried in the fiber, which highly limits its applications for *in vivo* detections. The scheme of coating nanoparticles on the inner surfaces of the air holes of the HCPCFs has not fully taken advantage of the light energy inside the fiber for SERS detection since it only utilized the power near the walls. Also, the photonic bandgap (PBG) may be lost when all of the air holes are filled with liquid, which may degrade the light confinement inside the fiber. In addition, the quality of HCPCF needs to be improved to have fewer defects, lower insertion loss, and better modal confinement.

2.2. LCPCF Probe. To overcome the problems mentioned above, a LCPCF probe was proposed and demonstrated [32]. The LCPCF was fabricated by sealing the cladding holes of the HCPCF while leaving the central core channel open. The SERS substrate, in this case SNPs, is mixed with the analyte instead of being coated on the walls. By dipping the sealed end of the HCPCF into the solution of SNPs/analyte, only the central core was filled due to the capillary effect. The transmission spectrum and the cross-section of the HCPCF in this experiment are shown in Figures 3(a) and 3(b). The HCPCF has a central core with a diameter around 6 μm while the cladding holes with a side length of 0.75 μm are arranged in a triangular lattice with a 1.6 μm pitch distance. A segment of 10 cm HCPCF was prepared with both ends carefully cleaved, and the cladding holes were sealed by inserting 2-3 mm of one tip of the HCPCF into a high-temperature flare ($\sim$1000°C) for 3–5 s. Figures 3(c) and 3(d) show that only the surrounding cladding holes were closed and the central core was still open. After cooling the fiber down for 5 min, the processed tip was dipped into the solution for 5 s, allowing the solution to fill the central core by $\sim$1 cm via capillary force and making it a LCPCF probe.

The schematic of LCPCF is shown in Figure 4, in which the excitation light was coupled into the unsealed end of the LCPCF and was confined in the core during propagation. After interacting with the mixed solution near the sealed end of the LCPCF, the SERS signal propagated back through the fiber to the unsealed end and then was collected by the spectrometer. A diode laser with 785 nm excitation wavelength was employed in the experiment to avoid damaging biomolecules. Sample measurements were performed under a Renishaw micro-Raman spectrometer with a Leica microscope a 50x objective lens.

Various sample solutions including Rhodamine 6G (R6G), human insulin, and tryptophan were prepared, separately, and each mixed with the SNPs colloid to test the LCPCF probe's sensitivity. The final concentrations of the sample solutions were 10^{-4}-10^{-5} M. In order to compare the sensitivity between the LCPCF probe and the previous HCPCF probe [31], we measured the background of the HCPCF (Figure 5(a), curve A) and used the HCPCF probe to detect R6G SERS signal (Figure 5(a), curves B and C). Similar experiments were conducted for human insulin and tryptophan solutions with HCPCF probe but no SERS signals were observed. By using a LCPCF probe, SERS measurement were performed for human insulin and tryptophan again. Figures 5(b) and 5(c) show that SERS signals from both of them were obtainable and consistent with those reported in the literature [39, 40]. This experiment demonstrates that the LCPCF sensor is more sensitive than the HCPCF probe, and this is attributed to the better confinement of both light and sample in the central core of the LCPCF and thereby increased interaction volume. A detailed quantitative analysis was also discussed in [32].

2.3. Inner Wall-Coated LCPCF Probe. In our earlier work, a double SERS substrate "sandwich" structure for fiber sensors was shown to enhance the SERS sensitivity [41]. The key idea of the "sandwich" structure is to use two types of SNPs as SERS substrates simultaneously; the stronger electromagnetic field between closely spaced SNPs is expected to greatly improve the SERS sensitivity based on the simulation work by Xu and Käll [42]. In our original design, one type of SNPs was coated on the tip of the normal multimode fiber and the other was mixed with the analyte in the sample solution. With the demonstration of higher sensitivity using the sandwich structure in multimode fiber sensor, we proposed an inner wall-coated LCPCF to combine the LCPCF probe with the sandwich structure [33].

The schematic of the inner wall-coated LCPCF probe is shown in Figure 6. One type of SNPs was coated on the inner surface of the central hollow core. The other type of SNPs was mixed with the analyte in the sample solutions. The solution entered into the hollow core from one end of fiber via the capillary action. Statistically, some of the molecules will be sandwiched in the junction between the two types of SNPs, where a stronger electromagnetic field leads to the enhanced SERS signal.

In this experiment, the LCPCF fabrication procedure was also modified. A fusion splicer was used to seal the cladding holes for better control of the process. By changing the arc power, arc duration, and positions of the fiber, the fusion splicer can generate heat more uniformly and seal the cladding holes more exactly than the previous flame method.

An injector was implemented to coat the SNPs onto the inner surface of the central core of HCPCF. With the HCPCF mounted inside a syringe and a sticky tape to close the gap between the syringe needle and the fiber, one end of the fiber was dipped into the SNPs solution and the injector was pulled to pump the SNPs into the core of the fiber. After the hollow core was filled with the SNPs, the fiber was dried for 20 min in order to remove the organic component from the SNPs. The coating procedure was repeated for several times to form a multilayer of SNPs on the inner surface of the fiber.

R6G was chosen as the test molecule with a concentration of 10^{-6} M. The solution was prepared by adding the analyte solution to the SNPs colloid. After incubated for about 10 min at room temperature, the solution was added with

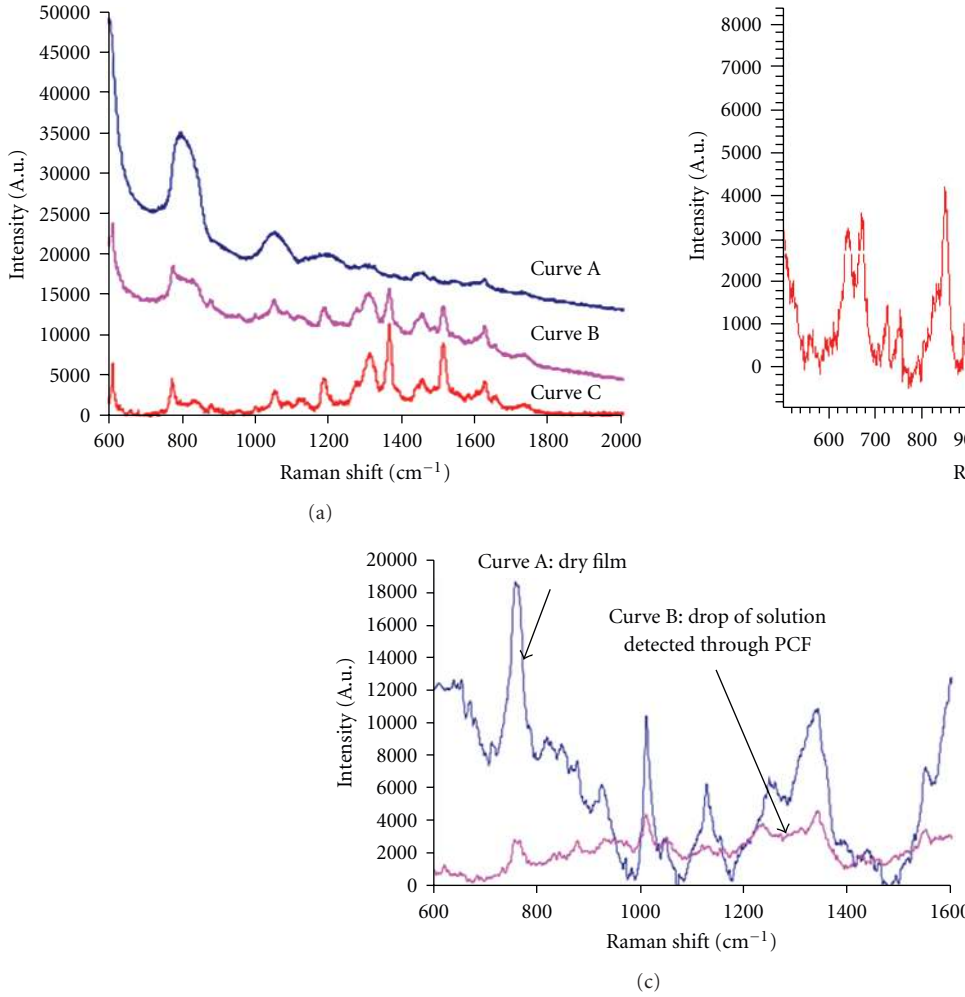

Figure 5: (a) Curve A: background Raman spectrum of the HCPCF. Curve B: R6G Raman spectrum obtained using a HCPCF SERS probe without the postfabrication processing; the HCPCF was dipped into the nanoparticle/R6G solution. Curve C: subtraction of Curve A from Curve B showing the net R6G Raman signal. (b) Human insulin SERS spectrum obtained using a LCPCF SERS probe after the postfabrication processing. The fiber background has been subtracted. (c) Comparison of SERS intensities between tryptophan obtained from the postprocessed LCPCF SERS probe and that obtained directly from a dried nanoparticle/analyte film.

sodium chloride (10 mM) to induce aggregation of SNPs for optimum SERS performance. Raman measurements were performed about 20 min after the introduction of salt.

Two different approaches were used for detecting the sample molecules in the inner wall-coated LCPCF. One way was the previous unsealed end detection, in which the laser light was coupled onto the unsealed end and propagated toward the sealed end to interact with the SERS sample solution. The other was the sealed end detection, in which the sealed end was placed under the microscope for coupling.

The experimental results are shown in Figure 7. Both the unsealed and sealed end detections achieve much better SERS signals than that obtained by directly focusing the excitation beam into the same mixed solution (direct sampling). Specifically, the signal obtained from the unsealed end is about 10 times stronger than that obtained from the direct sampling and the signal from the sealed end is around 100 times stronger than that from the direct sampling. Comparing the results of unsealed end detection of the inner wall-coated LCPCF with the previous LCPCF probe without coating [32], which is slightly higher than that from the direct sampling, it is obvious that sandwich structure indeed further increases the SERS signal. Moreover, it is interesting to observe that the signal from the sealed end is 10 times stronger than that from the unsealed end, which makes it a highlysensitive SERS probe. Motivated by the high sensitivity of the LCPCF SERS probe, our later work focuses on the investigation of the possible reasons for this high sensitivity and also attempts to push for much lower concentration detection.

2.4. Liquid-Filled HCPCF Probe. To quantitatively analyze the sensitivity enhancement introduced by the HCPCF, SERS experiments were performed with the liquid-filled HCPCF probes. For the liquid-filled HCPCF probes, one end of the HCPCF was cleaved carefully with a fiber cleaver and the other end was cut using a razor blade. The HCPCF used

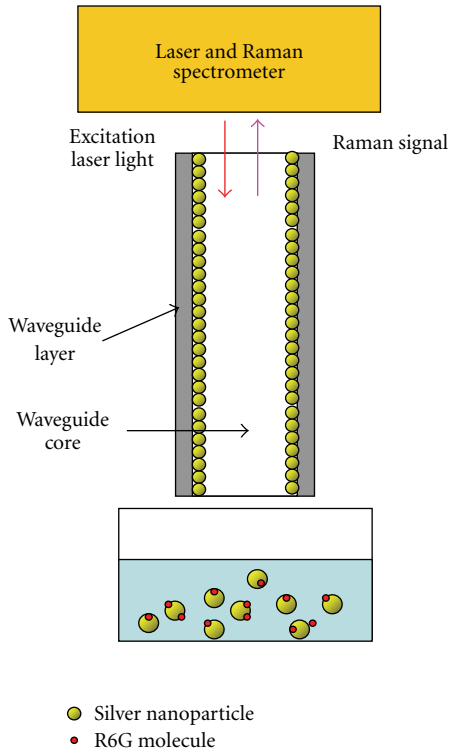

Figure 6: Schematic of the inner wall-coated LCPCF sensor.

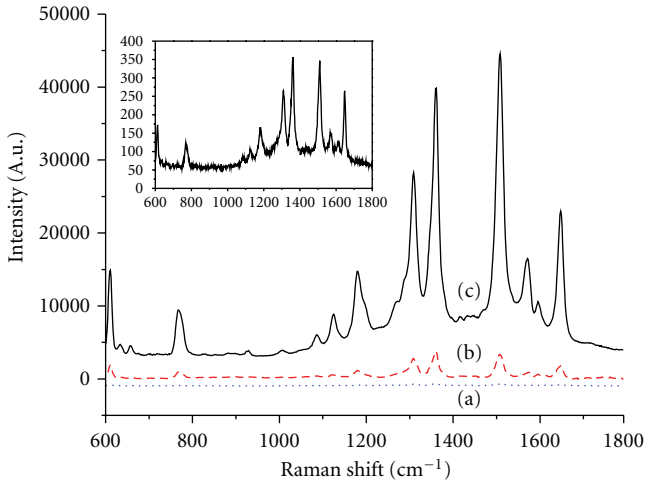

Figure 7: SERS spectra comparison of R6G molecules at the concentration of 10^{-6} M by using direct sampling and coated LCPCF: (a) direct sampling, (b) coated LCPCF detected from the unsealed end, and (c) coated LCPCF detected from the sealed end; inset: the enlarged SERS spectrum of direct sampling.

in the experiment is the same as that shown in Figure 3, and the length of the fiber varied from 2 mm to 5 cm. The cleaved end of the HCPCF segment was dipped into the mixed sample/SNPs solution and the liquid would fill both the central core and the surrounding cladding holes. Similar to the sealed end detection in Section 2.3, the dipped flat end was placed under the microscope for coupling. The Raman

Table 1: Using the 1509 cm^{-1} peak as an example, the intensity of the conventional Raman signal and the SERS signal in both the direct sampling and the liquid-filled HCPCF.

	Raman intensity (A.U.)	SERS intensity (A.U.)
Direct sampling	3104	3213
Liquid-filled HCPCF	190105	312946

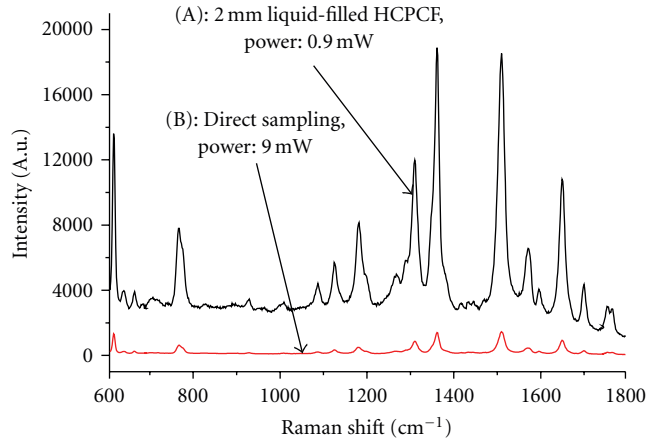

Figure 8: Comparison of SERS spectra of R6G at the concentration of 10^{-6} M between direct sampling and using a 2 mm liquid-filled HCPCF.

experiments were performed using a Renishaw InVia Raman Microscope system with a 632.8 nm excitation laser. A 50x objective lens was used to focus the excitation light into the HCPCF and also to collect the SERS signal.

Figure 8 shows the comparison of the SERS spectrum obtained from a 2 mm liquid-filled HCPCF with that from the direct sampling. The tested R6G concentration was 10^{-6} M in this experiment. Considering that the excitation power in the liquid-filled HCPCF is one 10th of that in the direct sampling, a 100-time sensitivity enhancement was observed for the liquid-filled HCPCF with a length as short as 2 mm.

To further explore the sensitivity enhancement of HCPCF, both conventional Raman and SERS experiments were conducted for comparison. The concentration of R6G was 4.18×10^{-2} M for the Raman experiment and 10^{-6} M for the SERS experiment. Choosing the intensity of the Raman peak at 1509 cm^{-1} as a reference, the sensitivity enhancement is 61 in the conventional Raman experiment and 97 in the SERS experiment as shown in Table 1. This experiment indicates a similar electromagnetic field distribution inside the liquid-filled HCPCF with and without SNPs, except for the difference in absorption coefficients.

Although the liquid-filled HCPCF can provide a sensitivity enhancement of 100 at relatively high concentration, it is found that at relatively low concentration, for example, 10^{-8} M R6G and 3.77×10^{-11} M SNPs, this approach cannot detect any SERS signal, which is buried by the strong

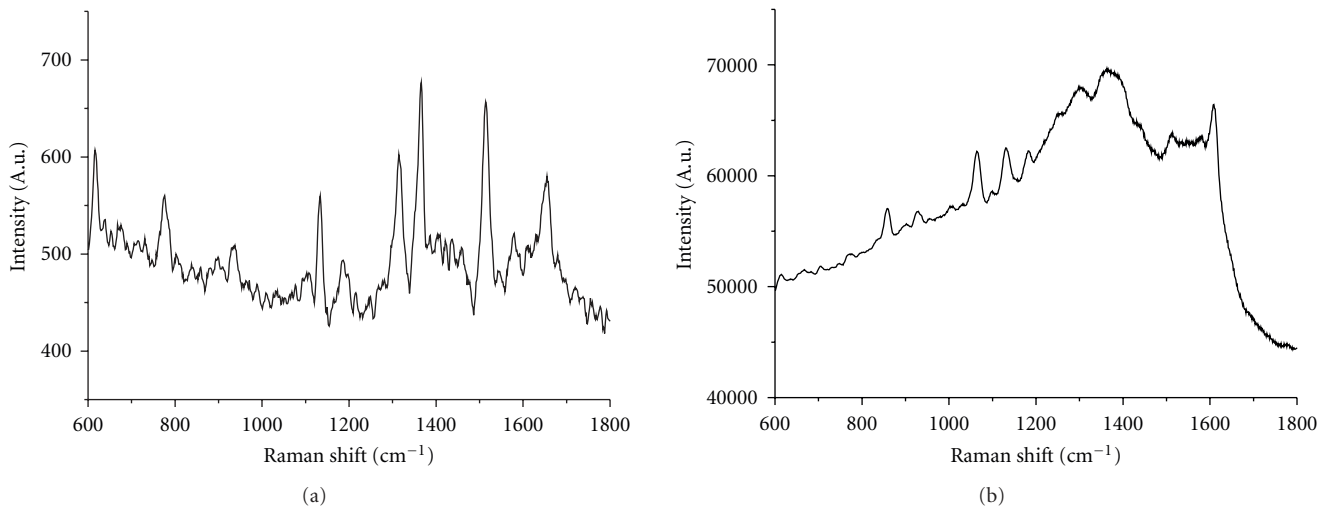

Figure 9: SERS signals detected from (a) direct sampling and (b) liquid-filled HCPCF when the concentration of R6G is 10^{-8} M. While direct sampling can detect R6G signal, liquid-filled HCPCF failed due to an enhanced SNPs background.

background, as shown in Figure 9. Since this background is significantly different from the Raman background of the silica [43], it is believed to be from the fluorescence and Raman spectra of the SNPs enhanced by the liquid-filled HCPCF.

The liquid-filled HCPCF experiments provide the information for theoretical analysis of the sensitivity enhancement of HCPCF, which will be shown in detail in Section 3. However, the problem of the large background has to be overcome in order to push for lower concentration detection.

2.5. Modified Highly Sensitive LCPCF Probe. In order to reduce the background, we used a slightly modified LCPCF SERS probe [34]. The preparation of the LCPCF was similar to that in Section 2.3, but the arc current used here (58 mA) was larger than that used previously (53 mA). This is to ensure all the cladding holes are sealed, especially the ones closest to the central core and to minimize the background from the claddings.

With the modified LCPCF filled with the mixed sample solution and placed under the microscope of the Raman spectrometer, the lowest detectable R6G concentration using the 3.77×10^{-11} M silver colloid was 10^{-10} M (0.1 nM) as shown in Figure 10. In this experiment, the SNP background is indeed reduced comparing to the results in the liquid-filled HCPCF probes. Although the exact mechanism of the background is still under investigation, we believe that it is related to the SNPs adhered to the silica surface. As the SNP decorated silica surface area in the liquid-filled HCPCF is much larger than that in LCPCF, the modified LCPCF results in a reduced SNP background.

It is also interesting to note that some of the SERS peaks split into two separate peaks (peaks d, e, g, and h) at this low concentration level. One possible reason is that at low concentrations, the R6G molecules are attached to the surface of the LCPCF in an ordered orientation/conformation,

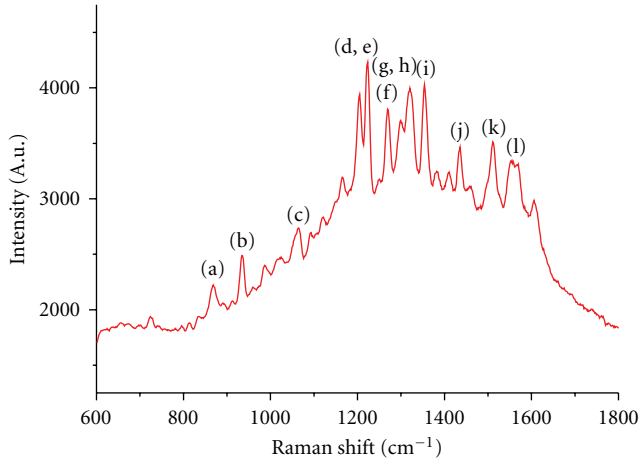

Figure 10: SERS signal from the detection of 0.1 nM R6G using a LCPCF. Peaks (a) and (c) are from the citrate introduced during the synthesis of SNPs. Peaks (b), (d), (e), (f), (g), (h), (i), (j), (k), and (l) are typical R6G peaks. Specifically, (d) and (e) are split from the 1204 cm^{-1} peak while (g) and (h) are split from the 1312 cm^{-1} peak compared to the high concentration SERS spectrum.

which gives narrower Raman peaks and the appearance of the two separate peaks; while at higher concentrations, besides those molecules adsorbed on the wall, there are some in the solution with a more random or inhomogeneous orientation/conformation, which result in inhomogeneously broadened Raman peaks and the appearance of one broad peak. Besides the R6G SERS peaks marked, other peaks (a and c) in Figure 10 can be attributed to citrate introduced during synthesis [44, 45].

It should be noticed that comparing to the results in Section 2.2, the performance of LCPCF SERS probe was significantly improved. And this improvement can be mainly

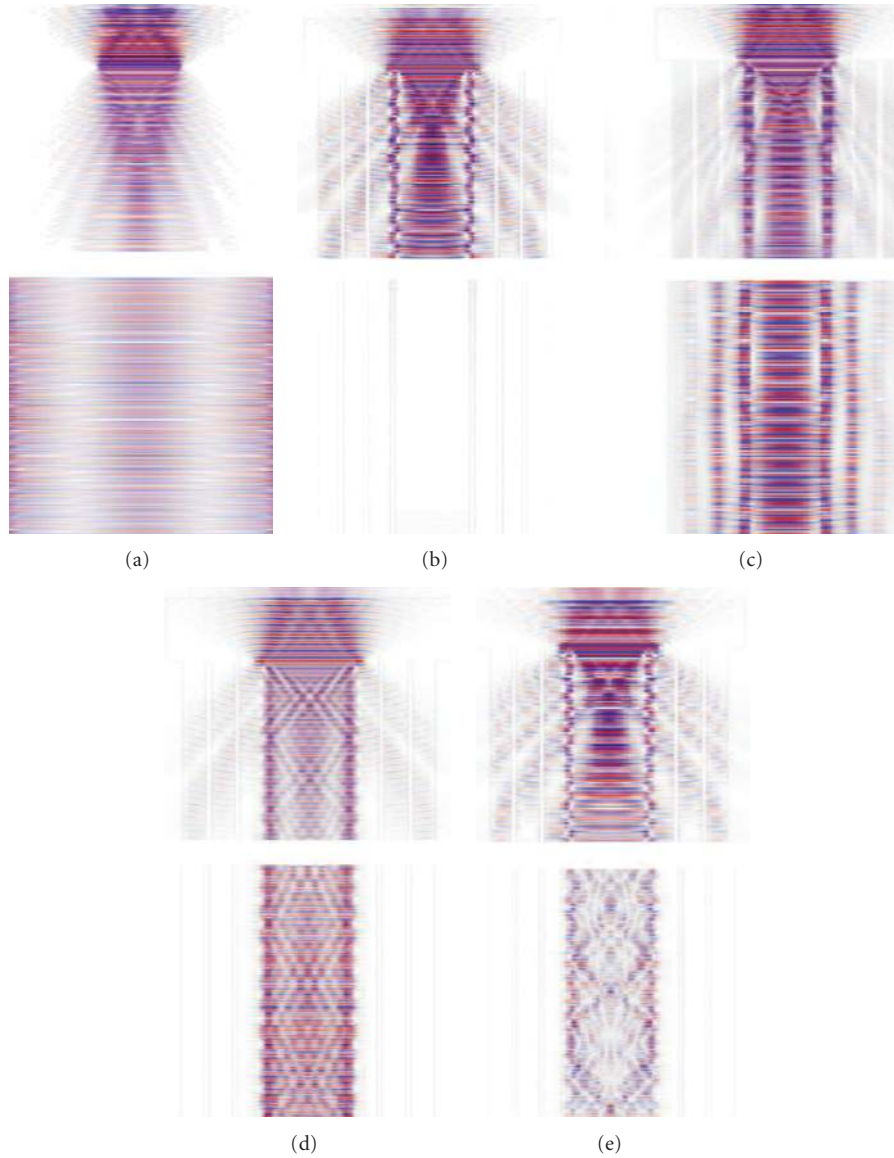

Figure 11: Light propagation when focusing a Gaussian beam at (a) the surface of a bulk liquid medium (water), (b) the entrance of a HCPCF with open air channels, (c) the entrance of a HCPCF with all channels filled with liquid, (d) the entrance of a LCPCF with only the core channels filled with liquid, and (e) the entrance of a LCPCF with a 200 μm air gap between the entrance and the liquid surface. In each set of images, the top one corresponds to the field distribution near the entrance of either bulk medium or HCPCF, while the bottom one corresponds to the field distribution after a propagation distance of 400 μm from the entrance.

attributed to the following two factors: a fusion splicer was used to seal all the cladding holes for better control of the process, and sealed end detection provides higher sensitivity than unsealed end detection if the liquid filling does not reach all the way to the top of the unsealed end.

3. Theoretical Analysis

To quantitatively explain the observed experimental results, especially the high sensitivity of HCPCF probes, we theoretically analyze the light distribution inside a HCPCF with the MIT MEEP code [46]. It is found that the liquid inside the air channels of the HCPCF significantly helps the light confinement inside the fiber even when the wavelength of the excitation light (e.g., 633 nm) does not match the designed transmission wavelength range of the HCPCF (745–853 nm).

In the simulation, we excited a Gaussian beam with a wavelength of 633 nm and a width of 6 μm, which was incident upon either a bulk liquid or a HCPCF. And the HCPCF had either open air holes, or all the holes filled with the liquid, or only the central core filled with the liquid, corresponding to the various experimental cases. The simulated HCPCF had the following parameters: the core diameter 4.5 μm, the side length of cladding holes 0.75 μm, pitch distance between cladding holes 1.6 μm, and three layers of cladding holes were considered.

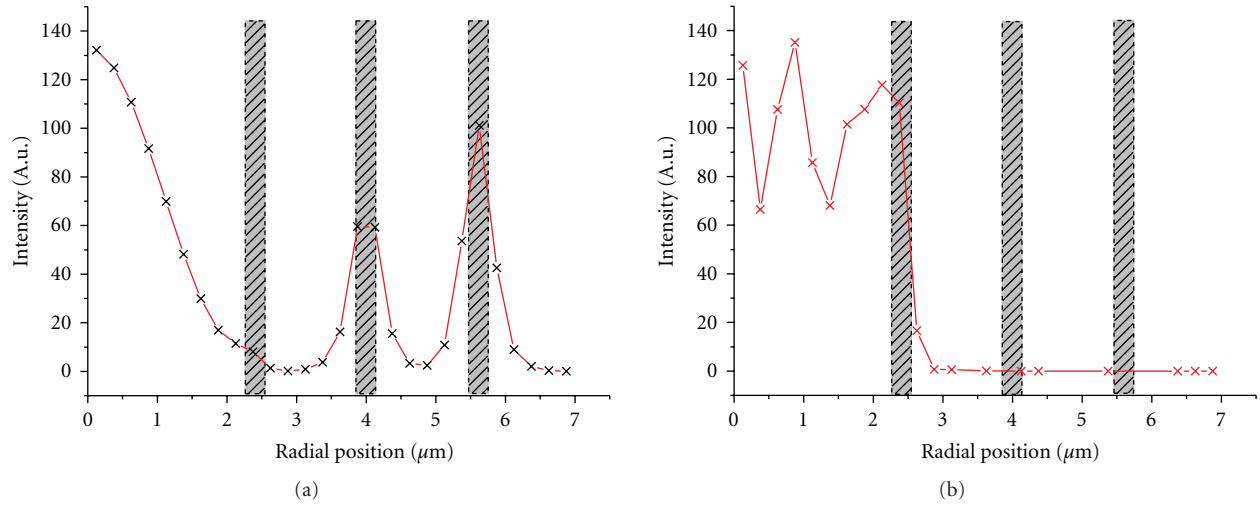

FIGURE 12: Plot of intensity distribution with respect to the radial position of (a) liquid-filled HCPCF and (b) LCPCF. Gray regions indicate silica walls in the PCF.

Figure 11 illustrates the light propagation in various cases: focusing a Gaussian beam at (a) the surface of a bulk liquid (water), (b) the entrance of a HCPCF with open air channels, (c) the entrance of a HCPCF with all channels filled with liquid, (d) the entrance of a LCPCF with only the core channels filled with liquid, and (e) the entrance of a LCPCF with a 200 μm air gap between the entrance and the liquid surface. Figure 11(a) represents the direct sampling and shows a decay of the light energy with propagation. Figure 11(b) shows that most power will be lost shortly during the propagation, since the excitation wavelength does not match the design wavelength range of the HCPCF. Figure 11(c) represents the liquid-filled HCPCF and shows that the light will decay very slowly after coupled into the fiber. This demonstrates the liquid significantly broadens the transmission range and provides the desired light confinement inside the fiber. Figure 11(d) represents the LCPCF and shows a similar light confinement but with much fewer light energies in the cladding areas. Figure 11(e) represents the unsealed end detection of the LCPCF probe, in which an air gap between the liquid surface and the fiber entrance may exist inside the fiber and will lead to a significant power loss. This can explain a lower sensitivity enhancement of unsealed end detection compared to the sealed end detection.

Figure 12 shows the intensity distribution with respect to the radial position in both the liquid-filled HCPCF and the LCPCF where the cross-section is 400 μm below the fiber entrance. Consistent with the result shown in Figure 11(c), Figure 12(a) indicates that although most of the light is inside the fiber core, a considerable light energy is propagating inside the glass regions of the cladding holes (shaded areas in Figure 12). The strong intensity of the evanescent wave near the walls results in an enhanced SNP background during the liquid-filled HCPCF experiments. Although the intensity near the wall of the fiber core in the LCPCF probe is still strong, the total effective interaction wall areas is much smaller than that in liquid-filled HCPCF, which results in a much weaker background.

Based on the simulation shown above, we compare the number of SERS particles in a liquid-filled HCPCF probe with that in the direct sampling to explain the mechanism behind the sensitivity enhancement and our experimental results. For a liquid-filled HCPCF probe, we consider the central core plus the nearest three cladding layers as the SERS-active regions. For the direct sampling, we consider the SERS-active region inside a cylinder with a Gaussian waist as the cross-section and the depth of focus as the effective length. Using the parameters of HCPCF in Section 2.2 and considering the shortest experimental length with a 100 times sensitivity enhancement that is 2 mm, the total number of nanoparticles/molecules in the interaction volume of a liquid-filled HCPCF is calculated to be 46 times that in a direct sampling, close to the sensitivity enhancement of 61 measured in Section 2.4 for the conventional Raman scattering. In addition, since the nanoparticles tend to adhere to the cladding walls where the evanescent wave is stronger, a redistribution of the light energy and nanoparticles results in an extra sensitivity enhancement in SERS experiments. These factors combined together contribute to an overall SERS sensitivity enhancement of 97 as shown in Section 2.4.

In addition to the above analysis, we also performed FDTD simulations for the electromagnetic field near particles inside a HCPCF and no significant field enhancement was observed. The FDTD result further confirms that the sensitivity enhancement is mainly due to the increased number of nanoparticles involved in the SERS activity.

4. Conclusions

Comparing with other SERS probes, the HCPCF probes have the following advantages: a high light intensity throughout the fiber propagation distance due to the confinement of light inside the HCPCF and a large interaction volume of

the nanoparticles and the analyte inside the air holes. It is found that the liquid inside the HCPCF helps confinement of the light, and, therefore, detection from the liquid-filled end has a better sensitivity. And although the liquid-filled HCPCF has a similar sensitivity enhancement as the LCPCF, an enhanced SNP background due to the interaction between the nanoparticles and the silica walls of the cladding holes may hinder detection at lower concentrations. And with SNPs as the SERS substrate and R6G as a test molecule, the lowest detectable concentration we have achieved is 10^{-10} M with a LCPCF probe, and 10^{-8} M for direct sampling. The high sensitivity provided by the LCPCF SERS probe makes it promising for molecular detection in various analytical and sensing applications.

Acknowledgments

The authors acknowledge the support from the National Science Foundation, ECCS-0823921, the UC MICRO grant, UARC/NASA, and the UCSC Special Research Grant.

References

[1] S. Weiss, "Fluorescence spectroscopy of single biomolecules," *Science*, vol. 283, no. 5408, pp. 1676–1683, 1999.

[2] E. A. Jares-Erijman and T. M. Jovin, "FRET imaging," *Nature Biotechnology*, vol. 21, no. 11, pp. 1387–1395, 2003.

[3] W. E. Moerner and D. P. Fromm, "Methods of single-molecule fluorescence spectroscopy and microscopy," *Review of Scientific Instruments*, vol. 74, no. 8, pp. 3597–3619, 2003.

[4] S. W. Hell, "Far-field optical nanoscopy," *Science*, vol. 316, no. 5828, pp. 1153–1158, 2007.

[5] K. Kneipp, H. Kneipp, I. Itzkan, R. R. Dasari, and M. S. Feld, "Ultrasensitive chemical analysis by Raman spectroscopy," *Chemical Reviews*, vol. 99, no. 10, pp. 2957–2975, 1999.

[6] K. E. Shafer-Peltier, C. L. Haynes, M. R. Glucksberg, and R. P. Van Duyne, "Toward a glucose biosensor based on surface-enhanced Raman scattering," *Journal of the American Chemical Society*, vol. 125, no. 2, pp. 588–593, 2003.

[7] A. Campion and P. Kambhampati, "Surface-enhanced Raman scattering," *Chemical Society Reviews*, vol. 27, no. 4, pp. 241–250, 1998.

[8] K. Kneipp, H. Kneipp, I. Itzkan, R. R. Dasari, and M. S. Feld, "Surface-enhanced Raman scattering and biophysics," *Journal of Physics: Condensed Matter*, vol. 14, no. 18, pp. R597–R624, 2002.

[9] H. Y. Chu, Y. Liu, Y. Huang, and Y. Zhao, "A high sensitive fiber SERS probe based on silver nanorod arrays," *Optics Express*, vol. 15, no. 19, pp. 12230–12239, 2007.

[10] S. Shanmukh, L. Jones, J. Driskell, Y. Zhao, R. Dluhy, and R. A. Tripp, "Rapid and sensitive detection of respiratory virus molecular signatures using a silver nanorod array SERS substrate," *Nano Letters*, vol. 6, no. 11, pp. 2630–2636, 2006.

[11] S. Nie and S. R. Emory, "Probing single molecules and single nanoparticles by surface-enhanced Raman scattering," *Science*, vol. 275, no. 5303, pp. 1102–1106, 1997.

[12] K. Kneipp, Y. Wang, H. Kneipp et al., "Single molecule detection using surface-enhanced Raman scattering (SERS)," *Physical Review Letters*, vol. 78, no. 9, pp. 1667–1670, 1997.

[13] T. A. Birks, P. J. Roberts, P. St. J. Russell, D. M. Atkin, and T. J. Shepherd, "Full 2-D photonic bandgaps in silica/air structures," *Electronics Letters*, vol. 31, no. 22, pp. 1941–1943, 1995.

[14] J. C. Knight, T. A. Birks, D. M. Atkin, and P. St. J. Russell, "Pure silica single-mode fiber with hexagonal photonic crystal cladding," in *Optical Fiber Communication Conference*, vol. 2 of *OSA Technical Digest Series*, Optical Society of America, San Jose, Calif, USA, 1996.

[15] R. F. Cregan, B. J. Mangan, J. C. Knight et al., "Single-mode photonic band gap guidance of light in air," *Science*, vol. 285, no. 5433, pp. 1537–1539, 1999.

[16] J. K. Ranka, R. S. Windeler, and A. J. Stentz, "Visible continuum generation in air-silica microstructure optical fibers with anomalous dispersion at 800 nm," *Optics Letters*, vol. 25, no. 1, pp. 25–27, 2000.

[17] F. Benabid, J. C. Knight, G. Antonopoulos, and P. St. J. Russell, "Stimulated Raman scattering in hydrogen-filled hollow-core photonic crystal fiber," *Science*, vol. 298, no. 5592, pp. 399–402, 2002.

[18] F. Benabid, J. C. Knight, and P. St. J. Russell, "Particle levitation and guidance in hollow-core photonic crystal fiber," *Optics Express*, vol. 10, no. 21, pp. 1195–1203, 2002.

[19] T. Ritari, J. Tuominen, H. Ludvigsen et al., "Gas sensing using air-guiding photonic bandgap fibers," *Optics Express*, vol. 12, no. 17, pp. 4080–4087, 2004.

[20] J. B. Jensen, L. H. Pedersen, P. E. Hoiby et al., "Photonic crystal fiber based evanescent-wave sensor for detection of biomolecules in aqueous solutions," *Optics Letters*, vol. 29, no. 17, pp. 1974–1976, 2004.

[21] S. Smolka, M. Barth, and O. Benson, "Selectively coated photonic crystal fiber for highly sensitive fluorescence detection," *Applied Physics Letters*, vol. 90, no. 11, Article ID 111101, 2007.

[22] S. Smolka, M. Barth, and O. Benson, "Highly efficient fluorescence sensing with hollow core photonic crystal fibers," *Optics Express*, vol. 15, no. 20, pp. 12783–12791, 2007.

[23] Y. Ruan, T. C. Foo, S. Warren-Smith et al., "Antibody immobilization within glass microstructured fibers: a route to sensitive and selective biosensors," *Optics Express*, vol. 16, no. 22, pp. 18514–18523, 2008.

[24] S. O. Konorov, C. J. Addison, H. G. Schulze, R. F. B. Turner, and M. W. Blades, "Hollow-core photonic crystal fiber-optic probes for Raman spectroscopy," *Optics Letters*, vol. 31, no. 12, pp. 1911–1913, 2006.

[25] D. Pristinski and H. Du, "Solid-core photonic crystal fiber as a Raman spectroscopy platform with a silica core as an internal reference," *Optics Letters*, vol. 31, no. 22, pp. 3246–3248, 2006.

[26] H. Yan, J. Liu, C. Yang, G. Jin, C. Gu, and L. Hou, "Novel index-guided photonic crystal fiber surface-enhanced Raman scattering probe," *Optics Express*, vol. 16, no. 11, pp. 8300–8305, 2008.

[27] A. Amezcua-Correa, J. Yang, C. E. Finlayson et al., "Surface-enhanced Raman scattering using microstructured optical fiber substrates," *Advanced Functional Materials*, vol. 17, no. 13, pp. 2024–2030, 2007.

[28] M. K. Khaing Oo, Y. Han, R. Martini, S. Sukhishvili, and H. Du, "Forward-propagating surface-enhanced Raman scattering and intensity distribution in photonic crystal fiber with immobilized Ag nanoparticles," *Optics Letters*, vol. 34, no. 7, pp. 968–970, 2009.

[29] M. K. Khaing Oo, Y. Han, J. Kanka, S. Sukhishvili, and H. Du, "Structure fits the purpose: photonic crystal fibers for evanescent-field surface-enhanced Raman spectroscopy," *Optics Letters*, vol. 35, no. 4, pp. 466–468, 2010.

[30] Y. Han, S. Tan, M. K. Khaing Oo, D. Pristinski, S. Sukhishvili, and H. Du, "Towards full-length accumulative surface-enhanced Raman Scattering-Active photonic crystal fibers," *Advanced Materials*, vol. 22, no. 24, pp. 2647–2651, 2010.

[31] H. Yan, C. Gu, C. Yang et al., "Hollow core photonic crystal fiber surface-enhanced Raman probe," *Applied Physics Letters*, vol. 89, no. 20, Article ID 204101, 2006.

[32] Y. Zhang, C. Shi, C. Gu, L. Seballos, and J. Z. Zhang, "Liquid core photonic crystal fiber sensor based on surface enhanced Raman scattering," *Applied Physics Letters*, vol. 90, no. 19, Article ID 193504, 2007.

[33] C. Shi, C. Lu, C. Gu et al., "Inner wall coated hollow core waveguide sensor based on double substrate surface enhanced Raman scattering," *Applied Physics Letters*, vol. 93, no. 15, Article ID 153101, 2008.

[34] X. Yang, C. Shi, D. Wheeler et al., "High-sensitivity molecular sensing using hollow-core photonic crystal fiber and surface-enhanced Raman scattering," *Journal of the Optical Society of America A*, vol. 27, no. 5, pp. 977–984, 2010.

[35] F. M. Cox, A. Argyros, M. C. J. Large, and S. Kalluri, "Surface enhanced Raman scattering in a hollow core microstructured optical fiber," *Optics Express*, vol. 15, no. 21, pp. 13675–13681, 2007.

[36] Y. Han, M. K. Khaing Oo, Y. Zhu et al., "Liquid-core photonic crystal fiber platform for Raman scattering measurements of microliter analyte solutions," in *Photonic Crystals and Photonic Crystal Fibers for Sensing Applications III*, vol. 6767 of *Proceedings of SPIE*, Boston, Mass, USA, September 2007.

[37] Y. Han, M. K. Khaing Oo, Y. Zhu et al., "Index-guiding liquid-core photonic crystal fiber for solution measurement using normal and surface-enhanced Raman scattering," *Optical Engineering*, vol. 47, Article ID 040502, 3 pages, 2005.

[38] J. Zhang, X. Li, X. Sun, and Y. Li, "Surface enhanced Raman scattering effects of silver colloids with different shapes," *Journal of Physical Chemistry B*, vol. 109, no. 25, pp. 12544–12548, 2005.

[39] S. K. Kim, M. S. Kim, and S. W. Suh, "Surface-enhanced Raman-scattering (SERS) of aromatic amino-acids and their glycyl dipeptides in silver sol," *Journal of Raman Spectroscopy*, vol. 18, pp. 171–175, 1987.

[40] L. Seballos, N. Richards, D. J. Stevens et al., "Competitive binding effects on surface-enhanced Raman scattering of peptide molecules," *Chemical Physics Letters*, vol. 447, no. 4–6, pp. 335–339, 2007.

[41] C. Shi, H. Yan, C. Gu et al., "A double substrate "sandwich" structure for fiber surface enhanced Raman scattering detection," *Applied Physics Letters*, vol. 92, no. 10, Article ID 103107, 2008.

[42] H. Xu and M. Käll, "Surface-plasmon-enhanced optical forces in silver nanoaggregates," *Physical Review Letters*, vol. 89, no. 24, Article ID 246802, 4 pages, 2002.

[43] J. Ma and Y.-S. Li, "Fiber Raman background study and its application in setting up optical fiber Raman probes," *Applied Optics*, vol. 35, no. 15, pp. 2527–2533, 1996.

[44] P. C. Lee and D. Meisel, "Adsorption and surface-enhanced Raman of dyes on silver and gold sols," *Journal of Physical Chemistry*, vol. 86, no. 17, pp. 3391–3395, 1982.

[45] M. Kerker, O. Siiman, L. A. Bumm, and D. S. Wang, "Surface enhanced Raman scattering (SERS) of citrate ion adsorbed on colloidal silver," *Applied Optics*, vol. 19, no. 19, pp. 3253–3255, 1980.

[46] A. Farjadpour, D. Roundy, A. Rodriguez et al., "Improving accuracy by subpixel smoothing in the finite-difference time domain," *Optics Letters*, vol. 31, no. 20, pp. 2972–2974, 2006.